정보저장시스템학회논문집, 제 5 권 제 1 호, pp. 19~35

회전원판 근처에서 회전하는 유연디스크에 대한 실험 및 수치해석

Experimental and Numerical Study on an Air-Stabilized Flexible Disk Rotating Close to a Rigid Rotating Disk

가드 압델라솔†, 임 윤철*

Abdelrasoul M. M. Gad and Yoon Chul Rhim

(2009 년 3 월 13 일 접수; 2009 년 3 월 19 일 심사완료; 2009 년 3 월 19 일 게재확정)

Abstract

The present work is an experimental and analytical study on a flexible disk rotating close to a rigid rotating disk in open air. In the analytical study, the air flow in the gap between the flexible disk and the rigid disk is modeled using Navier-Stokes and continuity equations while the flexible disk is modeled using the linear plate theory. The flow equations are discretized using the cell centered finite volume method (FVM) and solved numerically with semi-implicit pressure-linked equations (SIMPLE algorithm). The spatial terms in the disk equation are discretized using the finite difference method (FDM) and the time integration is performed using fourth-order Runge–Kutta method. An experimental test-rig is designed to investigate the dynamics of the flexible disk when rotating close to a co-rotating, a counter-rotating and a fixed rigid disk, which works as a stabilizer. The effects of rotational speed, initial gap height and inlet-hole radius on the flexible disk displacement and its vibration amplitude are investigated experimentally for the different types of stabilizer. Finally, the analytical and experimental results are compared.

Key Words : Flexible disk, rigid rotating disk, stabilizer, experimental study, Navier-Stokes equations, finite volume method

Nomenclature

r,θ,z	Cylindrical coordinates.
D	Bending stiffness of the disk material.
E	Young's modulus of the disk material.
F_P	Negative pressure force of the air-film.
F_C	Centrifugal force acting on the disk
F_S	Membrane forces due to stresses in disk.
F_B	Bending resistance force of the disk
h	Disk thickness.
h_o	Initial gap height.
J	Jacobian of transformation.
p	Fluid pressure.
p_a	Ambient pressure.
r	Radial distance.
r_o	Flexible disk outside radius.
r_c	Flexible disk clamping radius.
r_h	Inlet-hole radius.
Re_r, Re_θ, Re_z	Modified Reynolds numbers in radial, azimuthal and axial directions, respectively.
t	Time.
v_r, v_θ, v_z	Flow velocities along the coordinates directions.
v_r^o, v_θ^o, v_z^o	Reference velocities ($v_r^o, v_\theta^o, v_z^o = \omega\, r_o$).
w	Flexible disk displacement.
z	Axial distance.

Greek letters

η,ς,ξ	Computational coordinates.
∇^4	Biharmonic operator.
μ	Fluid viscosity.
υ	Poisson's ratio.
ρ	Fluid density.
ρ_d	Material density of the disk.
σ_r, σ_θ	Steady state stresses in the disk material in radial and circumferential directions.
ω	Angular velocity of the disk.

† 연세대학교 기계공학부
E-mail : gad76@yonsei.ac.kr
TEL : (02)2123-2820
* 연세대학교 기계공학부

1. Introduction

The rapid increase in information data calls for high-speed and reliable storage devices using small size and cheap media. Also, the strong demands for high data transfer rates results in high rotational speed of the media so that it is required to suppress the transverse vibration of the media as small as possible to read and write data successfully. Recently, the dynamics of rotating flexible disks are of a great interest due to its compactness as well as its low-cost. So, it is very important to investigate the design parameters for the flexible disk system since it is one of the good candidates for the next-generation high-capacity data storage devices. Several studies have been carried out for the investigation of the dynamic behavior of a thin, flexible disk, which is rotating close to a rigid plane, both analytically and experimentally.

Pelech and Shapiro [1] used an optical method to measure the gap distribution in radial direction between the rotating Mylar membrane and the rigid flat plane. Also, they analyzed the air flow in the gap numerically which is generated by the rotation of the membrane close to a rigid plane at low Reynolds number condition. One of their conclusions is that the gap distribution of the outer radius region is essentially independent from the clamping radius or the initial spacing between membrane and flat plane once the air flow rate is fixed.

Hosaka and Crandall [2] performed a single-mode analysis in order to obtain a rough estimate for the critical speed of a flexible disk coupled to thin air film in the gap. The onset speed of instability predicted by the single-mode analysis showed good agreement with the speed obtained from more accurate numerical method. They found that the instability appears when the relative velocity between the disk and the average air flow in the gap is larger than the velocity of the traveling wave of the disk vibration.

D'Angelo and mote [3] carried out thorough experiments on a thin steel disk rotating inside a cavity. The transverse motions of the disk were measured using inductance displacement transducers while the vibration frequencies were measured by spectral analyzer. They found that the disk spinning at supercritical rotational speed in a fluid becomes unstable due to the traveling wave aero-elastic flutter. Below the flutter speed, the disk vibrates under the unsteady pressure field due to the flow around the disk while at flutter or at higher speeds, the air flow is coupled with the disk motions. Also, they showed that a flat plane parallel to the disk with the gap of 0.5 cm does not change the flutter speed, frequency, or mode, rather it increases the post-flutter frequency.

Yasuda et al. [4] performed a theoretical as well as an experimental study for the self-excited vibrations of a flexible disk rotating in air. For the theoretical study, they analyzed the free vibrations of the disk with and without the effect of air. The forces produced by the air flow were considered in two terms; one is the ordinary viscous damping force and the other is the lifting force. The experimental study was conducted with a circular disk made of thin steel. The disk vibration was measured by using four sensors with 90 degrees apart. They concluded that the vibrations of the disk propagate as forward and backward traveling waves. They showed the backward traveling waves can have self-excited characteristics at rotational speeds higher than certain value while the forward traveling waves decay always.

Huang and Mote [5] investigated the instability mechanisms in the coupled fluid-disk system analytically. The air flow in the gap was modeled using a modified Reynolds equation that includes the contribution of the fluid inertia due to the circular motion while the transverse vibration of the disk was modeled as a classical rotating plate under the distributed air film pressure. They showed that the maximum rotational speed for the stable rotation of the disk is bounded by the lowest onset speed of rotating damping instability.

Lee et al. [6] investigated the aerodynamic coupling effect on the natural frequencies and flutter instabilities of rotating disks experimentally. The experiments were performed for two optical disks; CD and ASMO disks. The disk vibration was measured by using an LDV while the displacement signal was transferred to a dynamic analyzer. They investigated the behavior of the disk when rotating in open air, inside the cavity, and in vacuum chamber. They found that the natural frequencies of the disk increase due to the aerodynamic coupling between the disk and surrounding air in the post-flutter regions.

Naganthan et al. [7] performed a numerical study about the flutter instability of a flexible disk rotating close to a rigid plane. The disk was modeled using the linear plate theory while the flow in the gap was modeled using the classical Reynolds equation of lubrication considering the radial flow. They concluded that the rotating disk showed flutter instability, possibly self-excited vibrations, in the presence of air when the speed of rotation is above the critical speed for a given disturbance mode.

Onagi et al. [8] developed an optical disk system

using a flexible disk and an air stabilizer. They succeeded to reduce the axial run out of the disk within 5μm as a result of the aerodynamic effect of the stabilizer. Also, they demonstrated experimentally that they can record signals at a density of 0.13μm/bit while suppressing the axial run out of less than 5μm.

Recently, Aman et al. [9-11] developed a flexible optical disk (FOD) system composed with a flexible disk and three stabilizers, which can achieve small axial run out of the disk through simplified stabilizer control. They adopted new stabilizer system made up of triangularly arranged stabilizers (TAS) and demonstrated that it could effectively stabilize a flexible disk even under conditions with no active stabilizer adjustments, such as axial position control and tilt control, which could not be eliminated in their previous single-stabilizer system. Later, they improved their TAS design by changing the arrangement of the stabilizers asymmetrically. Then, they found experimentally that the asymmetrical design controls the aerodynamic stabilization of the disk more effectively, especially at a pickup focal point.

Kang and Raman [12, 13] carried out analytical and experimental studies about the vibrations and instabilities of a rotating disk coupled with acoustic oscillations of surrounding air. The analytical study showed that the presence of bulk rotating fluid flow increases the flutter speed for mode coalescence and splits all acoustic-dominated modes into forward and backward traveling waves. From the vibration measurement of the rotating disk, flutter instabilities of reflected traveling wave were observed at supercritical speeds and they claimed that the flutter instabilities observed in their experiment is not the mode coalescence but the damping-induced instabilities leading to the flutter of a single reflected traveling wave.

It can be noticed from the previous review that the earlier studies did not consider the effects of centrifugal force, inertia force, and Coriolis force due to air flow on the fluid-disk inter-acting behavior. These forces should be considered when investigating the dynamics of spinning flexible disks rotating at relatively high speeds. Also, previous studies focused their analyses as well as their experiments on a flexible disk rotating close to a fixed plane and no attempt was made to investigate the dynamics of the fluid disk system when the flexible disk is rotating close to a rigid co-rotating or counter-rotating plane. Since the critical speed of a stable disk vibration is bounded by the onset speed of the rotating damping instability [5], the critical speed of the disk can be increased significantly if the speed of the rotating damping relative to the disk is decreased by introducing a rotating stabilizer instead of the fixed one.

The present work is an experimental and analytical study on a flexible disk rotating close to a rotating rigid-plane in open air. The air flow in the gap between the flexible disk and the rigid plane is modeled using Navier-Stokes and continuity equations while the flexible disk is modeled using the linear plate theory. The flow equations are solved numerically using the FVM with the SIMPLE algorithm. The spatial terms in the disk equation are discretized using the FDM while time integration is performed using the fourth-order Runge–Kutta method. An experimental test-rig is designed to investigate the displacement and vibration amplitude of the flexible disk when it rotates close to a co-rotating, a counter-rotating, and a fixed plane, which is actually a disk made of glass and is called a stabilizer. Experiments are focused to investigate the effects of the rotational speed, the initial gap height between the flexible disk and the stabilizer at the clamping radius, and the inlet-hole radius through which air can flow in. Comparisons and discussions between the analytical and experimental results are followed.

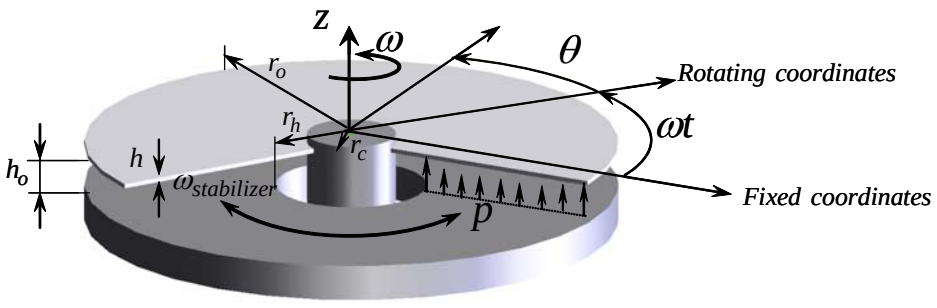

Fig. 1 Analytical model of the disk-fluid system.

2. Analytical Model

2.1 Flow equation

The details of the present numerical model were explained in a former work [14]. In the analytical model, the flow between the rotating flexible disk and the rotating rigid disk is modeled using Navier-Stokes and continuity equations in cylindrical co-ordinates. Figure 1 shows a schematic representation of the analytical model used in this study.

The model shows an annular disk which is clamped at its inner radius (r_c), is set free at its outer radius (r_o), and is rotating with the constant angular velocity (ω) above a rigid rotating disk separated by a distance (h_o). The air flow in the gap is assumed to be steady laminar flow and incompressible with constant viscosity. The Navier-stokes and continuity equations are expressed in dimensionless form in eqn. (1). The viscous terms in the order of $(h_o/r_o)^2$ are neglected since the gap height is very small compared with the disk radius. In the present study, the physical coordinates (r, θ, and z) are mapped into (η, ζ, and ξ) coordinates, respectively, in the computational domain. The dimensionless flow equations in the new computational domain considering the convective inertia force, the fluid Coriollis force, the fluid centrifugal force, the fluid viscous force, and the fluid pressure force are expressed as follows:

η-momentum equation:

$$Re_r \frac{1}{\eta}\frac{\partial \rho \eta v_r v_r}{\partial \eta} + Re_\theta \frac{1}{\eta}\frac{\partial \rho v_\theta v_r}{\partial \varsigma} + Re_z J \frac{\partial \rho v_z v_r}{\partial \xi} - Re_\theta \left(\frac{v_\theta^o}{v_r^o}\right)\frac{\rho v_\theta^2}{\eta} - Re_r Jz_\eta \frac{\partial \rho v_r v_r}{\partial \xi} - Re_\theta Jz_\varsigma \frac{1}{\eta}\frac{\partial \rho v_\theta v_r}{\partial \xi}$$
$$= -\left(\frac{p_a h_o^2}{\mu v_r^o r_o}\right)\left\{\frac{\partial p}{\partial \eta} - Jz_\eta \frac{\partial p}{\partial \xi}\right\} + \mu J^2 \frac{\partial^2 v_r}{\partial \xi^2}$$

ς-momentum equation:

$$Re_r \frac{1}{\eta}\frac{\partial \rho \eta v_r v_\theta}{\partial \eta} + Re_\theta \frac{1}{\eta}\frac{\partial \rho v_\theta v_\theta}{\partial \varsigma} + Re_z J \frac{\partial \rho v_z v_\theta}{\partial \xi} + Re_r \frac{\rho v_r v_\theta}{\eta} - Re_r Jz_\eta \frac{\partial \rho v_r v_\theta}{\partial \xi} - Re_\theta Jz_\varsigma \frac{1}{\eta}\frac{\partial \rho v_\theta v_\theta}{\partial \xi}$$
$$= -\left(\frac{p_a h_o^2}{\mu v_\theta^o r_o}\right)\frac{1}{\eta}\left(\frac{\partial p}{\partial \varsigma} - Jz_\varsigma \frac{\partial p}{\partial \xi}\right)\mu J^2 \frac{\partial^2 v_\theta}{\partial \xi^2}$$

ξ-momentum equation:

$$Re_r \frac{1}{\eta}\frac{\partial \rho \eta v_r v_z}{\partial \eta} + Re_\theta \frac{1}{\eta}\frac{\partial \rho v_\theta v_z}{\partial \varsigma} + Re_z J \frac{\partial \rho v_z v_z}{\partial \xi} - Re_r Jz_\eta \frac{\partial \rho v_r v_\theta}{\partial \xi} - Re_\theta Jz_\varsigma \frac{1}{\eta}\frac{\partial \rho v_\theta v_z}{\partial \xi}$$
$$= -\left(\frac{p_a h_o}{\mu v_z^o}\right) J \frac{\partial p}{\partial \xi} + \mu J^2 \frac{\partial^2 v_z}{\partial \xi^2}$$

Continuity equation:

$$Re_r \frac{1}{\eta}\frac{\partial \rho \eta v_r}{\partial \eta} + Re_\theta \frac{1}{\eta}\frac{\partial v_\theta}{\partial \varsigma} + Re_z J \frac{\partial v_z}{\partial \xi} - Re_r Jz_\eta \frac{\partial \rho v_r}{\partial \xi} - Re_\theta Jz_\varsigma \frac{1}{\eta}\frac{\partial \rho v_\theta}{\partial \xi} = 0 \qquad (1)$$

where, v_r, v_θ, and v_z are the flow velocities along radial, azimuthal, and axial coordinates, respectively, also Re_r, Re_θ, and Re_z are the modified Reynolds numbers along the coordinate directions and (J) is the Jacobian used in the coordinate transformation. The definitions of the other parameters are as explained in the nomenclature. An algebraic grid generation technique [15] is used to build up a uniformly staggered grid pattern after grid distortion due to disk deformation at every iteration cycle.

The flow equations in the computational domain are solved with the following boundary conditions; mass conservation at inlet-hole and outlet perimeter, zero radial and axial velocities at the flexible disk surface and no-slip boundary condition is used for the tangential velocity, zero radial and axial velocities at the stabilizer surface while the tangential velocity at the stabilizer surface depends on the type of stabilizer used (i.e. co-rotating, counter-rotating or fixed stabilizer); also periodic boundary conditions are used in the circumferential direction for the velocity components

and the pressure of the air film in the gap.

2.2 Disk equation

The disk is assumed to be thin ($h \ll r_o$) and the disk material is isotropic with Young's modulus (E), Poisson's ratio (υ) and density (ρ_d). The disk material is assumed to be linearly elastic so that Hook's law holds. Also, it is assumed that the in-plane displacements are negligibly small compared with the transverse deflections. As the disk is assumed to be very thin, the transverse deflection is assumed to be constant across the disk thickness. Two coordinate systems are used in the present analysis; the first is rotating with the disk (r, θ, and z), while the second coordinate system ((η, ζ, and ξ) is fixed in the space. The relation between the two coordinate systems is ($\varsigma = \theta + \omega t$). The linear elastic equation describing the small transverse displacement (w) of the thin spinning disk is given by:

$$\frac{1}{r}\frac{\partial}{\partial r}\left(r\sigma_r \frac{\partial w}{\partial r}\right)+\frac{1}{r}\frac{\partial}{\partial \theta}\left(\sigma_\theta \frac{1}{r}\frac{\partial w}{\partial \theta}\right)-\frac{D}{h}\nabla^4 w+\frac{p}{h}=\rho_d \frac{\partial^2 w}{\partial t^2} \quad (2)$$

Here, σ_r and σ_θ are the radial and circumferential steady state stresses in the disk due to the centrifugal force by rotation. Also, (D) represents the bending stiffness of the disk and (p) is the fluid pressure.

The disk equation is solved with the following boundary conditions; vanishing disk displacement and disk slope at the clamping radius and vanishing bending moment and shear force at the outer radius. Also, periodic boundary condition is used in circumferential direction for the disk displacement and axial velocity.

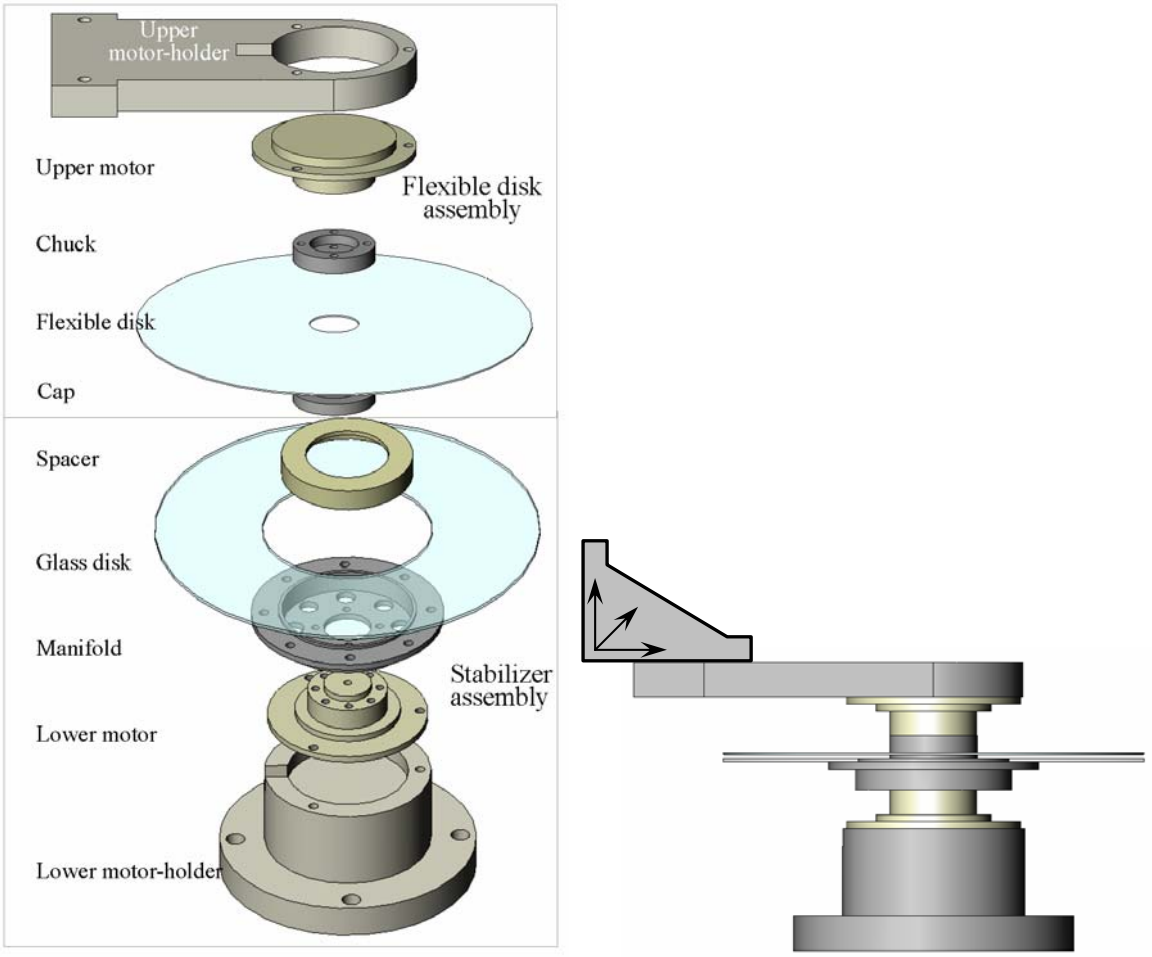

Fig. 2 Exploded and assembled views of the experimental test-rig

2.3 Numerical method

The flow equations are discretized using the cell-centered FVM on a uniformly staggered grid. The velocities at cell boundaries are approximated using the upwind differencing scheme. The discretized flow equations are solved with the semi-implicit pressure linked equations (SIMPLE) algorithm, Patankar [16], using the alternative direction implicit method with tri-diagonal matrix solver algorithm. The spatial terms in the disk equation are discretized using second order finite difference method while the temporal derivative is integrated using the fourth-order Runge-Kutta time marching scheme. In this numerical simulation, the pressure obtained from the iterative solution of the flow equations is used to calculate the disk displacement at the next time step. Then, the boundary conditions for the flow equations are updated and the numerical grid generation technique is used with the SIMPLE algorithm to calculate the new pressure field to be used for the next iteration cycle in disk equation. The process is repeated until the disk reaches a steady-state deflection determined by a certain convergence criterion that monitors the relative change of the air-film pressure between successive time steps.

3. Experimental set-up

In order to validate the analytical model, an experimental work is carried out to measure the effects of the rotational speed, the inlet-hole radius, and the initial gap height on the flexible disk displacement and its vibration amplitude. For this purpose, an experimental test-rig is designed to facilitate the aforementioned measurements. The stabilizer design should consider its main functions; co-rotating, counter-rotating, or fixed relative to the rotating flexible disk. In order to satisfy these requirements, the experimental test-rig is composed of two parts; the lower part is the stabilizer assembly while the upper part is the flexible disk assembly. The stabilizer assembly consists of the lower motor-holder, HDD motor, manifold, glass disk (acts as a rigid flat-stabilizer), and spacers for adjusting the inlet-hole size. The flexible disk assembly consists of the upper motor-holder, HDD motor, chucking system, and a polycarbonate flexible disk. An exploded as well as assembled view of the experimental test-rig is shown in Fig.2.

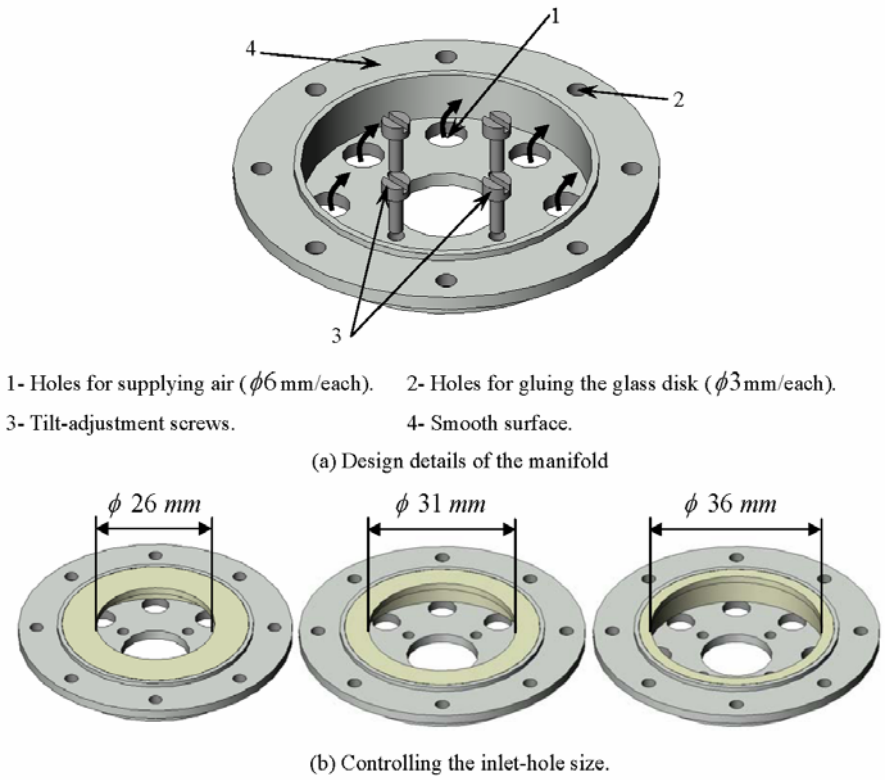

Fig. 3 Design details of the manifold to meet its functions.

The manifold of the stabilizer assembly has 8 holes of 6mm diameter per each to allow sufficient air supply at the inlet side as shown in Fig. 3(a). The manifold is glued to the glass disk, which has a mirror surface and is assumed perfectly flat. The thickness of the disk is 1.3mm, the inner diameter is 43mm, and the outer diameter is 120mm (same outside diameter of the flexible disk). Four screws are used to adjust the tilt of the glass disk after assembly. The tilt of the glass disk is adjusted within 5μm at r=58mm. The inlet-hole size is controlled by inserting spacers with different hole-sizes in the manifold cavity as shown in Fig. 3(b). The motor-shaft of the flexible disk assembly protrudes in the manifold cavity to ensure the concentricity check and initial gap-height control. Three spacers are used with inlet-hole radii of 13, 15.5 and 18mm to give radial clearances of 0.5, 3 and 5.5mm, respectively.

Table 1 Specifications of the laser displacement sensor.

Model	Keyence LK-G10
Reference distance	10mm
Measurement range	± 1mm
Light source	Red semiconductor laser (650 nm wavelength)
Resolution	0.02μm

The flexible disk assembly is attached to a system of micro-stages so that the axis of the flexible disk can be aligned vertically with that of the glass disk to assure the concentricity. The test-rig is assembled on a vibration isolation table and the displacement and its vibration amplitude of the flexible disk are measured using a laser displacement sensor that has the specifications given in Table 1.

Due to the geometry of the experimental test-rig and the size of the laser displacement sensor, the disk displacement is measured at five points in the radial direction (r=41, 46, 50, 54, and 58mm) and at three different angles in the circumferential direction. Since the steady state disk displacement of the disk should be axisymmetric, the displacement is approximated as the average of three displacement readings in circumferential direction at given radius.

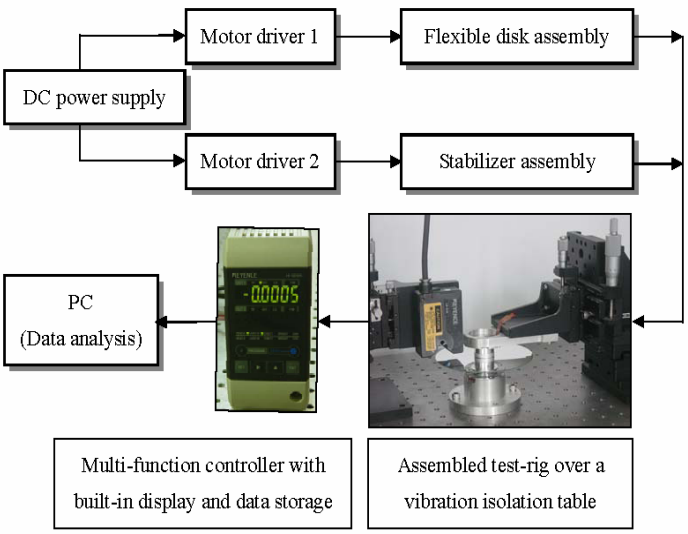

Fig. 4 Data acquisition chart

Table 2 Specifications of the polycarbonate flexible disk.

Outside radius r_o (mm)	Clamping radius r_c (mm)	Thickness h (mm)	Density ρ_d (kg/m^3)	Elasticity modulus E (GPa)	Poisson's ratio (υ)
60	12.5	0.095	1,200	2.5	0.23

Table 3 Experimental conditions with different stabilizers.

Measurement	Fixed stabilizer case	Co-rotating stabilizer case	Counter-rotating stabilizer case
Rotation speed effect	3,600, 5,400, and 7,200rpm		
Initial gap height effect	100, 150, 200, 250, and 300μm	100, 150, 200, 250, and 300μm	150, 200, 250, and 300μm
Inlet-hole size effect	r_h = 13.0, 15.5, and 18.0mm		

The power is supplied to the lower and upper HDD motors through the motor drivers 1 and 2 as shown in Fig. 4. In the experiments, the motor for flexible disk rotates in one direction and the polarity of the motor for stabilizer is changed to allow the stabilizer to co-rotate or counter-rotate relative to the direction of rotation of the flexible disk. The fixed stabilizer case is studied by temporarily gluing the HDD motor to the motor holder.
A flexible disk, which is made of polycarbonate, with the specifications given in Table 2 is used throughout the experiment. One side of the flexible disk, that faces the glass disk, is coated with a very thin silver film (60nm thick) at which the laser beam is reflected. Table 3 summarizes the experimental conditions.

4. Experimental results and discussions

4.1 Initial gap height effect

The effects of the initial gap height on the flexible disk displacement and its peak-to-peak vibration amplitude with different stabilizers are shown in Fig. 5. The rotational speed for the cases shown in Fig. 5 is 7,200rpm and the inlet-hole radius is 18mm. It can be noticed from Fig. 5(a) that the flexible disk displacement is directly proportional to the initial gap height, also the disk slope is very small at the investigated range ($41 \le r \le 58$ mm) and this agrees well with the numerical simulation results [14]. The small slope of the disk near the outer edge may be attributed to the large centrifugal force acting on the disk material at this region which acts to flatten the disk while the effect of the negative pressure force is almost negligible. The results from Fig. 5(b) show that the peak-to-peak vibration amplitudes of the flexible disk decrease with the decrease of the initial gap height. The reason for the decrease in vibration is the increase in stiffness of the air-film as well as its damping capability when the initial gap height decreases. Also, Fig. 5(b) shows clearly that the disk vibration increases towards the outer edge and this result agrees well with the numerical simulations of Hosaka and Crandall [2].

It is important to mention that, when using counter-rotating stabilizer, the rotation speed of 7,200rpm does not represent the absolute speed of the disk or the stabilizer rather it represents the disk speed relative to the stabilizer. The disk rotates at 6,000rpm while the stabilizer rotates at 1,200rpm in the opposite direction so that the speed of the disk relative to the stabilizer is 7,200rpm.

4.2 Rotational speed effect

The effects of the rotation speed on the flexible disk displacement and its peak-to-peak vibration amplitude with different stabilizers are shown in Fig. 6. The initial gap height for the cases shown here is 200μm and the inlet-hole radius is 15.5mm.

It can be noticed from Fig. 6(a) that the flexible disk displacement increases slowly with the increase of the rotational speed. Also, this behavior agrees well with the numerical simulation results [14].

The behavior of the flexible disk can be explained as follows; the increase in disk rotational speed increases the centrifugal force acting on the gas molecules and thereby increases the negative pressure force of the air-film (F_P) that acts to pull the disk towards the stabilizer. However, at the same time, increasing the rotational speed of the disk increase the centrifugal forces acting on the disk material (F_C) and the membrane forces associated with stresses in the disk (F_S). Thus, the increase in the negative pressure force is accompanied by a corresponding increase in the resisting disk-material forces; hence the disk displacement is not affected much with the increase in the rotational speed of the disk.

Figure 6(b) shows that the peak-to-peak vibration amplitude of the flexible disk when rotating close to a fixed stabilizer decreases with the increase in the rotational speed of the disk while the peak-to-peak vibration amplitude of the flexible disk rotating close to a co-rotating stabilizer increases with the increase in the rotational speed of the disk. The reason for these different behaviors of the disk may be understood if we consider that the increase in rotational speed when the disk rotates close to a fixed stabilizer or a co-rotating stabilizer increases the resisting forces of the disk-material (F_C and F_S) with the same amount in both cases, but the increase in air-film force due to the negative pressure (F_P) for the co-rotating stabilizer case is much more than that of the fixed stabilizer case. The resisting

disk-material forces besides the disk resistance to bending (F_B) act to flatten the disk while the negative pressure force acts to deflect the disk towards the stabilizer. Thus, for the fixed stabilizer case, the increase of the negative pressure force is balanced by the corresponding increase of the resisting disk-material forces and this results in the decrease of the disk lateral vibration while the large increase in negative pressure force for the case of co-rotating stabilizer is not balanced and this results in the increase of the disk lateral vibration.

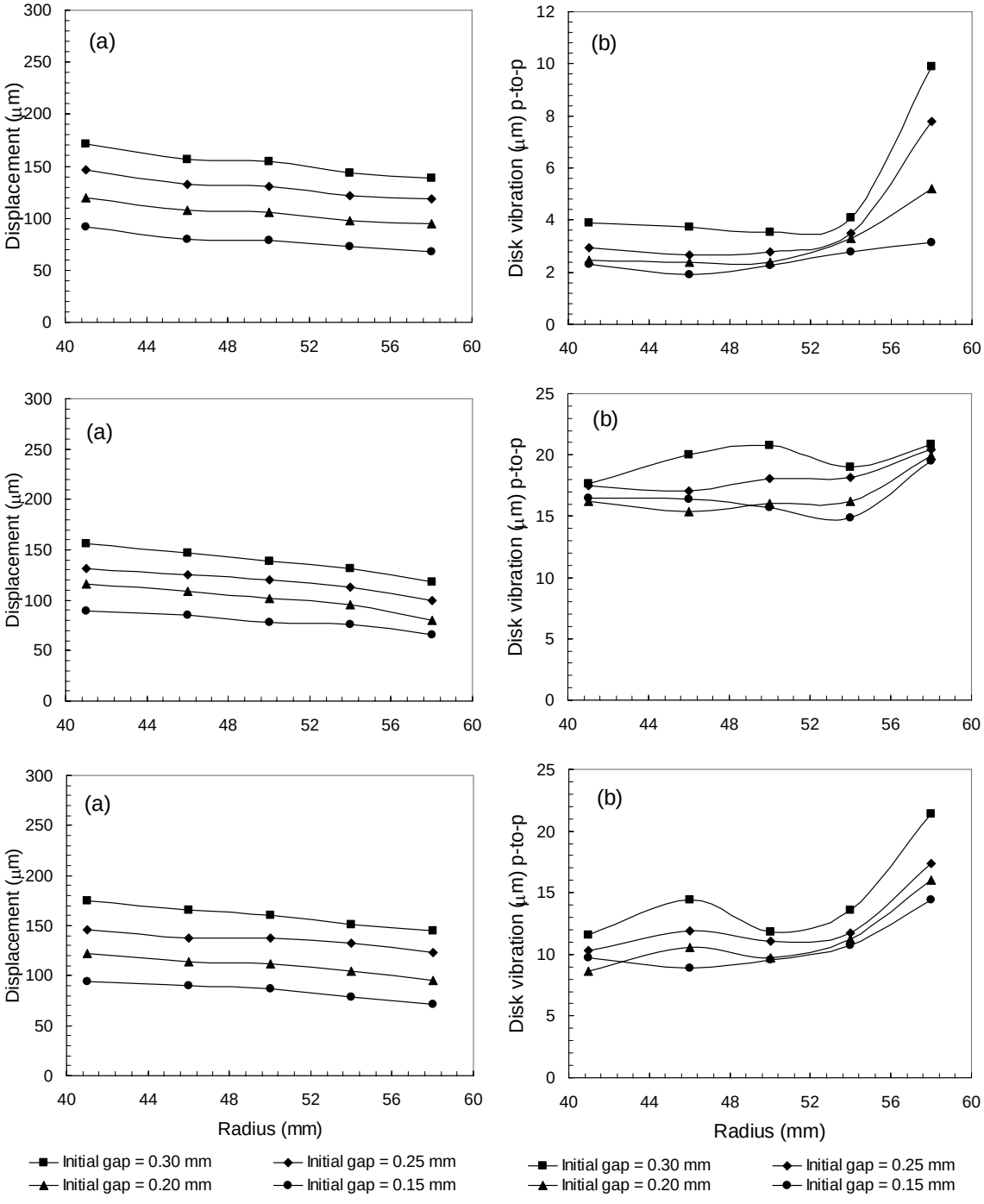

Fig. 5 Initial gap height effect on the flexible disk with different stabilizers ($\omega = 7200$ rpm, $r_h = 18$ mm): (a) Flexible disk displacement. (b) Peak-to-peak vibration amplitude.

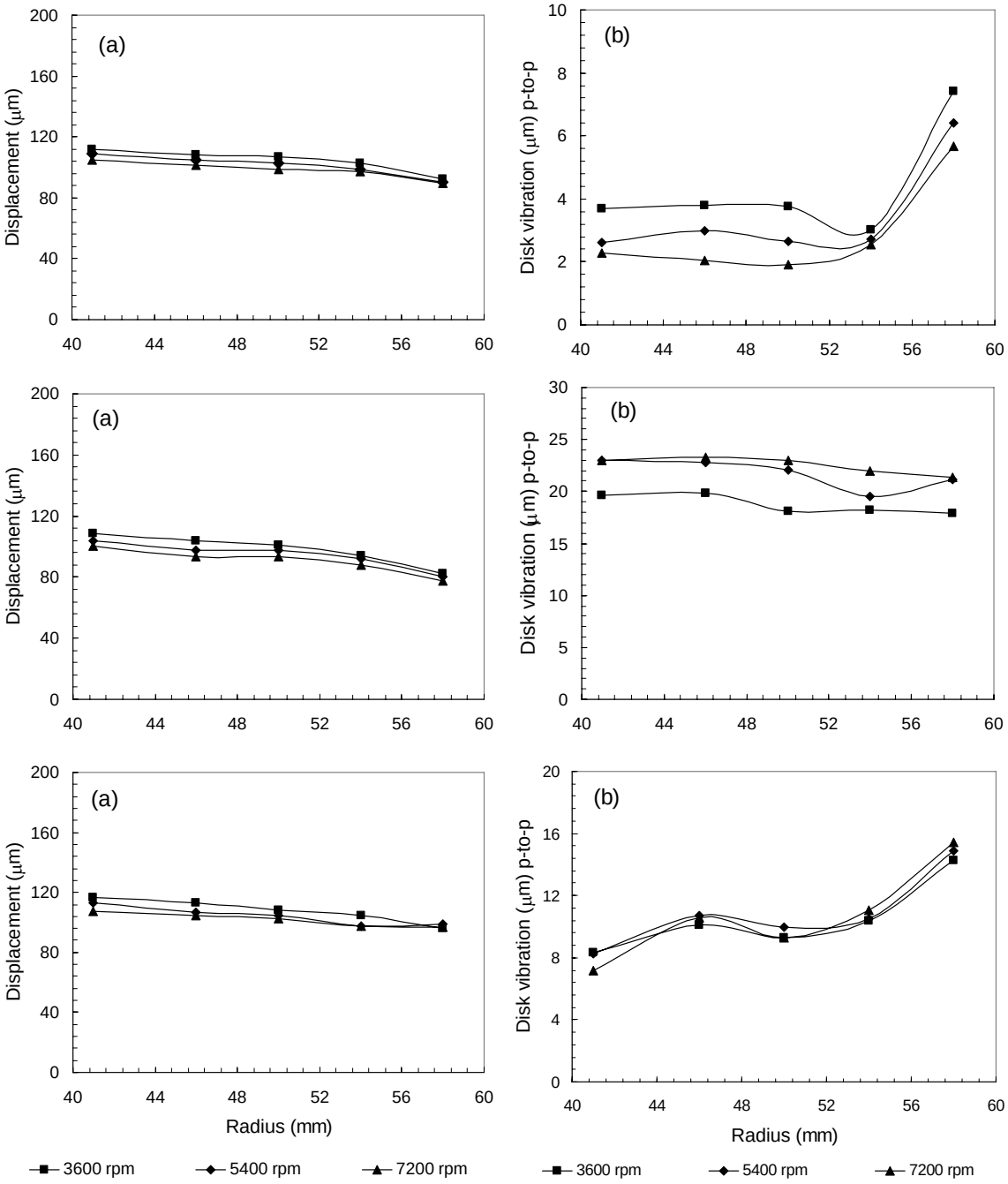

Fig. 6 Rotational speed effect on the flexible disk with different stabilizers ($h_o = 200\ \mu\text{m}, r_h = 15.5$ mm): (a) Flexible disk displacement. (b) Peak-to-peak vibration amplitude.

Also, it can be noticed from Fig. 6(b) that the effect of rotational speed on the flexible disk vibration, when rotating close to a counter-rotating stabilizer, is not significant and the disk vibration increases towards the outer edge of the disk. This trend is similar to the result for the fixed stabilizer.

4.3. Inlet-hole radius effect

The effects of the inlet-hole radius on the flexible disk displacement and its peak-to-peak vibration amplitude with different stabilizers are shown in Fig. 7. The initial gap height for the cases shown here is 200μm and the rotational speed is 7,200rpm. It is noticeable from Fig. 7(a) that the flexible disk displacement increases when the inlet-hole radius is decreased. The reason for this behavior is the increase of the negative pressure force due to the continuous outward flow without sufficient compensation from the inlet hole. Also,

this conclusion agrees well with that obtained from the numerical simulations [14].

Figure 7(b) shows that the vibration amplitude of the disk rotating close to a fixed or a counter-rotating stabilizer at the inlet-hole radius of 15.5mm is smaller than that at the inlet-hole radii of 13mm or 18mm. This behavior of the disk shows clearly that narrow as well as wide inlets are not good candidates for the proper design of such systems. However, Fig. 7(b) shows that the flexible disk behaves in a different way when rotating close to a co-rotating stabilizer; the peak-to-peak vibration amplitude of the flexible disk rotating close to co-rotating stabilizer decreases with the increase of the inlet-hole radius. The behavior of the flexible disk near a co-rotating stabilizer may be interpreted as follows:

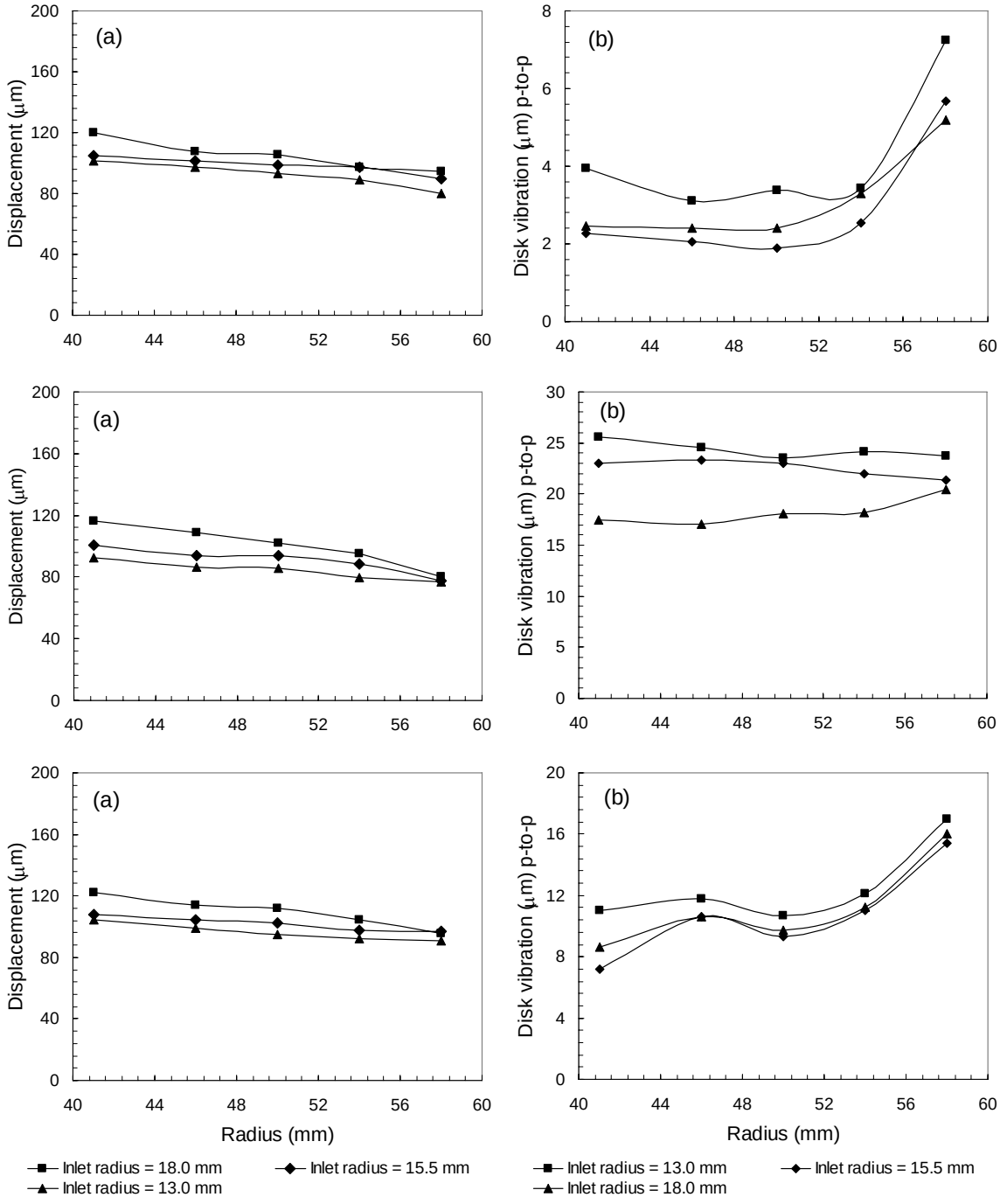

Fig. 7 Inlet-hole radius effect on the flexible disk with different stabilizers ($\omega = 7200$ rpm, $h_o = 200$ μm): (a) Flexible disk displacement. (b) Peak-to-peak vibration amplitude.

When the inlet-hole radius decreases, the negative pressure force increases and consequently the air-film losses most of its stiffness and damping capabilities that leads to the increase the lateral vibration of the disk. By increasing the inlet-hole radius, the negative pressure force is reduced until it is being balanced by the resisting disk-material forces and consequently the air-film recovers its stiffness and damping capabilities that result in the decrease of the flexible disk vibration. However, it should be expected that the increase of the inlet-hole radius beyond some limit will also lead to excessive disk vibration as the air-film stiffness and damping will decrease due to the decrease or even the absence of the balancing negative pressure force in the air-film.

4.4. Comparison of flexible disk behavior with different stabilizers

Comparisons of the flexible disk behavior with fixed, counter-rotating and co-rotating stabilizers at inlet-hole radii of 13, 15.5 and 18mm are given in Figs. 8, 9 and 10, respectively; the initial gap height is 300μm and the rotational speed is 7,200 rpm. Two conclusions can be drawn out from Figs. 8(a), 9(a) and 10(a); the first is that the flexible disk displacement with a counter-rotating stabilizer is the smallest relative to that with a fixed and a co-rotating stabilizers. The second is that the difference between the flexible disk displacements with the three kinds of stabilizers becomes more considerable as the inlet-hole radius increases.

It is clear from Figs. 8(b), 9(b), and 10(b) that the vibration amplitude of the flexible disk rotating close to a co-rotating stabilizer is the highest among the three kinds of stabilizers and the vibration amplitude of the disk with a counter-rotating stabilizer becomes closer to that with a co-rotating stabilizer as the inlet-hole radius increases. The reason for the relatively small displacement of the disk with a counter-rotating stabilizer is that the presence of a counter-rotating wall reduces the centrifugal force acting on the gas molecules and thereby reduces the negative pressure force of the air film that acts to pull the disk towards the stabilizer. Also, the presence of the counter-rotating wall creates a shear plane in the gap between the rotating disk and the counter-rotating wall which in turn increases the stiffness of the air-film to resists the lateral vibration of the disk.

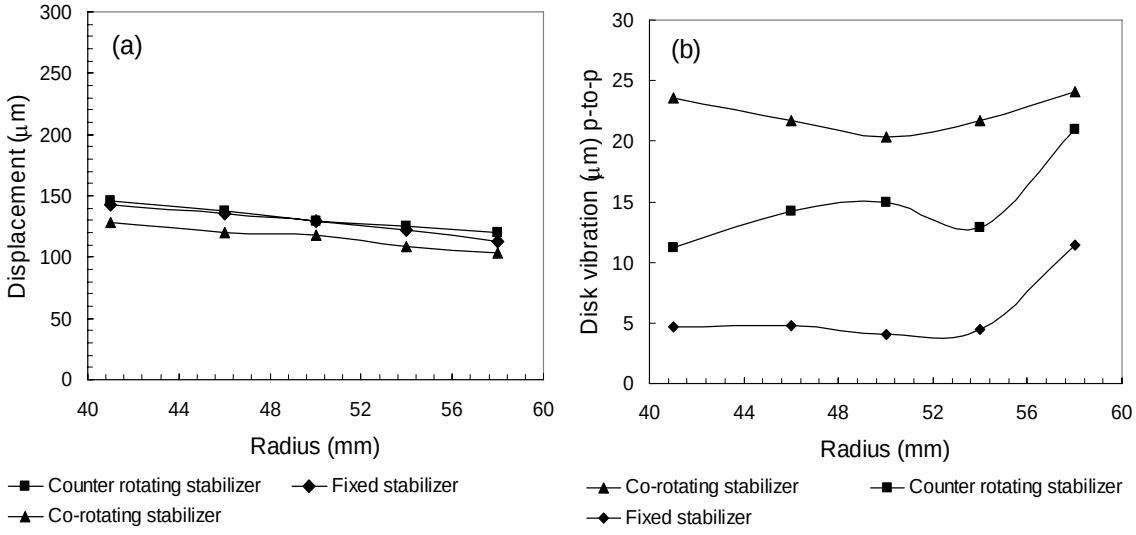

Fig. 8 Comparison between the flexible disk behavior with fixed, counter-rotating and co-rotating stabilizer ($\omega = 7200$ rpm, $h_o = 300$ μm, $r_h = 13$ mm): a) Flexible disk displacement. (b) Peak-to-peak vibration amplitude.

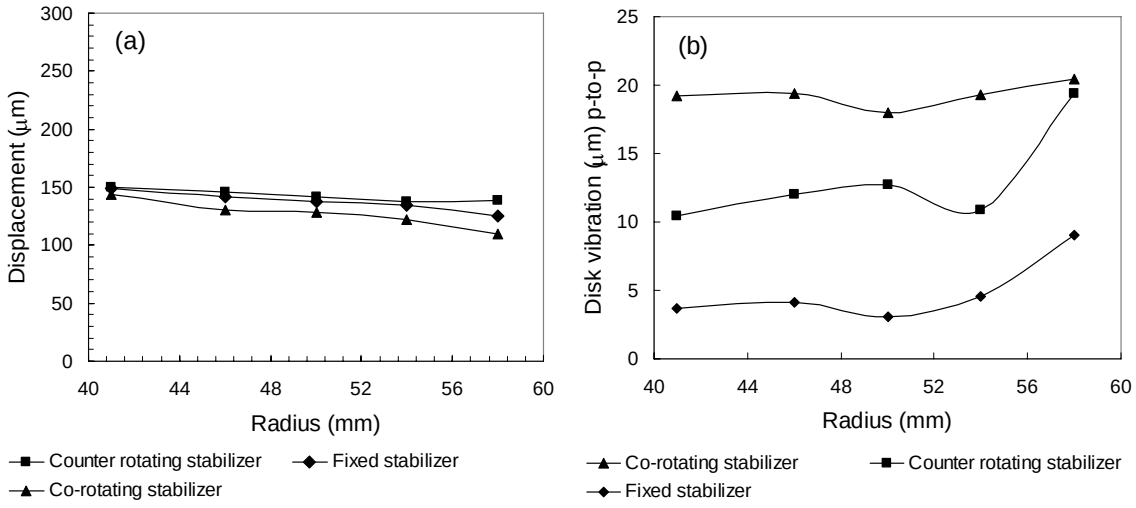

Fig. 9 Comparison between the flexible disk behavior with fixed, counter-rotating and co-rotating stabilizer ($\omega = 7200$ rpm, $h_o = 300$ μm, $r_h = 15.5$ mm): a) Flexible disk displacement. (b) Peak-to-peak vibration amplitude.

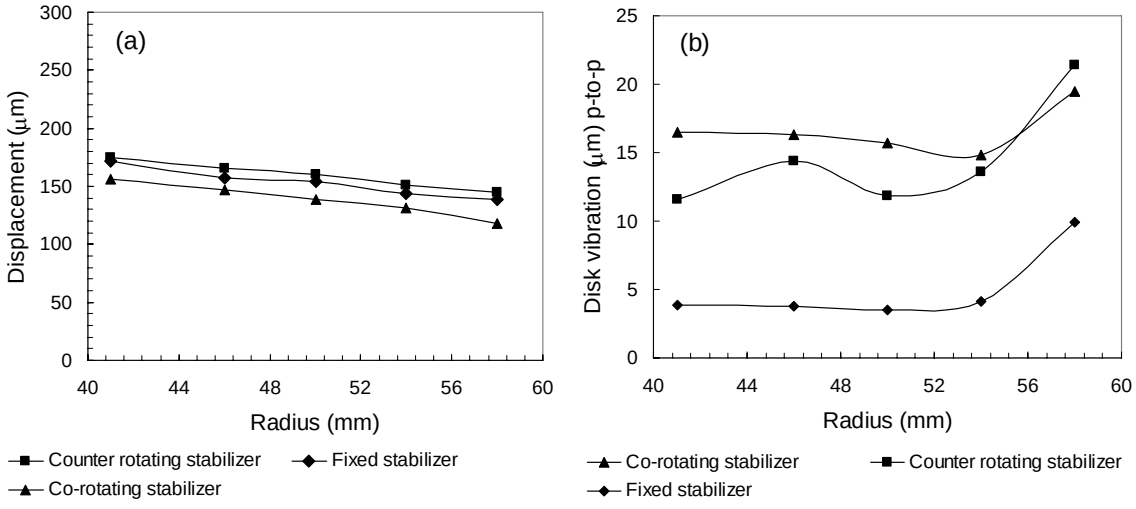

Fig. 10 Comparison between the flexible disk behavior with fixed, counter-rotating and co-rotating stabilizer ($\omega = 7200$ rpm, $h_o = 300$ μm, $r_h = 18$ mm): a) Flexible disk displacement. (b) Peak-to-peak vibration amplitude.

5. Comparison between experimental and numerical results

In this section, the experimental conditions (i.e. the rotational speed of the flexible disk, the rotational speed of the stabilizer, the inlet-hole radius, the initial gap height, the flexible disk properties, etc) are substituted into the developed numerical code and the results from the numerical simulations are compared with those obtained from the experimental investigations.

A comparison between the experimental and numerical flexible disk displacements with different stabilizers is shown in Fig. 11 where the initial gap height and the inlet-hole radius are 200μm and 13mm, respectively.

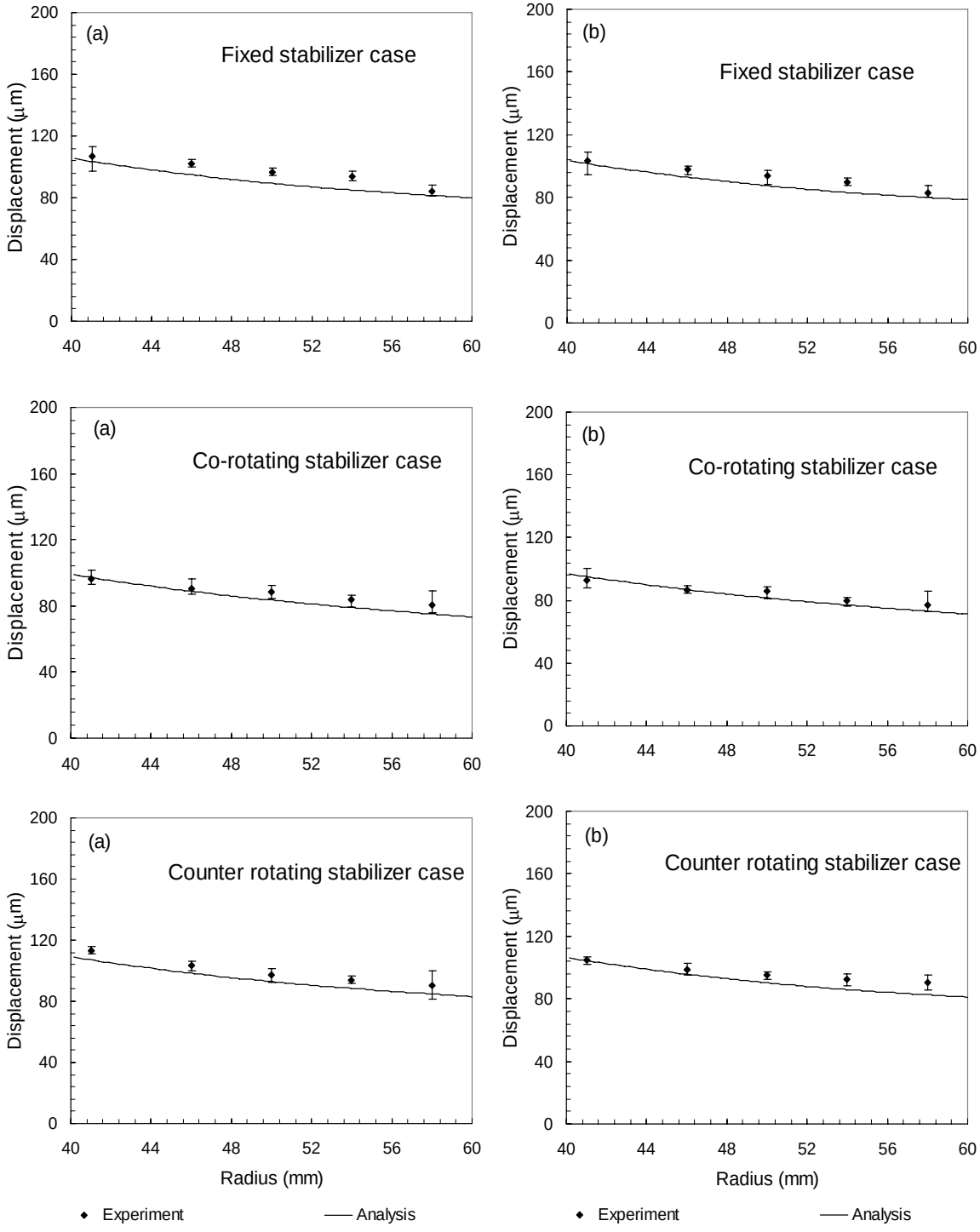

Fig. 11 Comparison between experimental and numerical results through the flexible disk displacement ($h_o = 200\ \mu\text{m}, r_h = 13$ mm): (a) ω=5,400rpm. (b) ω=7,200rpm.

The error bars shown in the figures represent the maximum and minimum values of the measured displacement at the specified point (as the displacement was measured at three different positions in the circumferential direction). The figures show clearly that the experimental results agree well with the numerically obtained results at the investigated region of the disk.

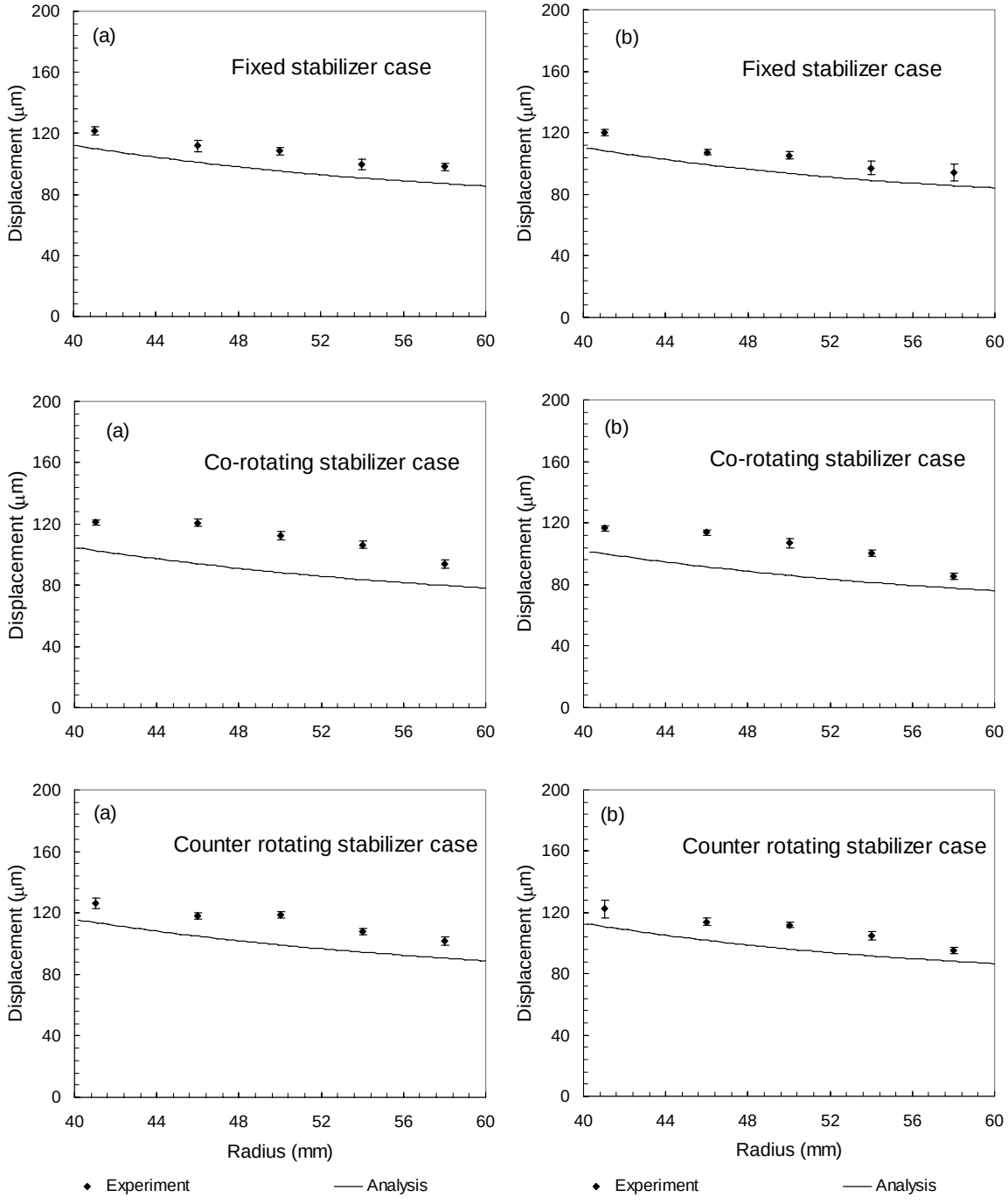

Fig. 12 Comparison between experimental and numerical results through the flexible disk displacement ($h_o = 200\ \mu\text{m}, r_h = 18$ mm): (a) ω=5,400rpm. (b) ω=7,200rpm.

Another comparison between the experimental and numerical flexible disk displacements with different stabilizers is shown in Fig. 12 where the initial gap height and the inlet-hole radius are 200μm and 18mm, respectively. It can be noticed from the figures that the predicted numerical displacements are lower than those obtained experimentally. Thus it can be concluded that the developed numerical code overestimates the flexible disk displacements at large inlet-hole radii while it gives a reasonable estimation for the flexible disk displacement with different stabilizers at small inlet-hole radius. In other words, the numerical analysis overestimates the negative pressure force of the air-film at large inlet-hole radii.

The reason for the difference between the flexible disk displacements obtained experimentally and those obtained from the numerical simulation at large inlet-hole radius can be explained as follows: For the numerical simulations the domain of calculations is very thin relative to its radial length (the steady state thickness of the air film is less than 0.1 mm while the radial length is 47.5mm. i.e. $r_o/h > 470$). Thus any changes at the inlet propagate very slowly in the radial direction and eventually the outer region is not affected much with such changes at the inlet. The situation is quite different in the real system because the air-film thickness changes momentarily (increases/decreases) allowing any changes at the inlet to affect the whole domain.

6. Conclusions

The present work introduces experimental and numerical study about the dynamic behavior of a flexible disk rotating close to a co-rotating, a counter-rotating, and a fixed flat stabilizer. The flow in the gap between the spinning disk and the rigid stabilizer is modeled using Navier-Stokes and continuity equations while the disk is modeled using the linear plate theory. The flow equations are discretized with the FVM and solved using SIMPLE algorithm while the spatial terms in the disk model are discretized using FDM and time integration is performed using the fourth-order Runge-Kutta method. An experimental device was designed to measure the effects of the rotational speed, the inlet-hole radius, and the initial gap height on the flexible disk displacement and the lateral vibration. The following conclusions can be drawn out from the present work:

- The peak-to-peak vibration amplitude of the flexible disk decreases with the decrease of the initial gap height for the different kinds of stabilizers.

- The flexible disk displacement increases slightly with the increase in the rotational speed and this conclusion agrees well with that obtained from the numerical simulations [14].

- The peak-to-peak vibration amplitude of the flexible disk rotating close to a fixed stabilizer decreases with the increase in the rotational speed of the disk while the peak-to-peak vibration amplitude of the flexible disk rotating close to a co-rotating stabilizer increases with the increase in the rotational speed.

- The flexible disk displacement increases when the inlet-hole radius is decreased for the different kinds of stabilizers.

- Narrow as well as wide inlets are not good candidates for the proper design of flexible disk systems rotating close to a fixed or a counter-rotating stabilizer.

- The peak-to-peak vibration amplitude of the flexible disk rotating close to a co-rotating stabilizer decreases with the increase of the inlet-hole radius.

- The results from the experimental investigations show that the flexible disk displacement with the counter-rotating stabilizer is the smallest relative to the other types of stabilizers and the difference between the flexible disk displacements with the three kinds of stabilizers becomes more considerable as the inlet-hole radius increases.

- The vibration amplitude of the flexible disk rotating close to a co-rotating stabilizer is the highest among the three kinds of stabilizers and the vibration amplitude of the disk with a counter-rotating stabilizer becomes closer to that with a co-rotating stabilizer as the inlet-hole radius increases.

- The developed numerical code overestimates the flexible disk displacement at large inlet-hole radii while it gives a reasonable estimation at small inlet-hole radius for the studied stabilizers.

Acknowledgements

This work was supported by the Korea Research Foundation; Grant funded by the Korea Government (MOEHRD), (KRF-2006-211-D00013). The authors gratefully thank Mr. Nobuaki Onagi (RICOH Company, Ltd. Japan) for the careful preparation of the polycarbonate flexible disks; without his kind cooperation this work would not be completed.

References

[1] Pelech, I., and Shapiro, A. H., 1964, “Flexible disk rotating on a gas film next to a wall”, ASME Journal of Applied Mechanics, Vol. 31, pp.577 – 584.

[2] Hosaka, H. and Crandall, S. H., 1992, “Self – excited vibrations of a flexible disk rotating on an air film above a flat surface”, Acta Mechanica (Suppl.) 3: pp.115 – 127.

[3] D’Angelo C. and Mote, C. D. JR, 1993, “Aerodynamically excited vibration and flutter of a thin disk rotating at supercritical speed”, Journal of Sound and Vibration, Vol.168 (1), pp.15 – 30.

[4] Yasuda, K., Torii, T., and Shimizu, T., 1992, “Self-excited oscillations of a circular disk rotating in air”, JSME International Journal, series III, Vol. 35, No. 3, pp.347 – 352.

[5] Huang, F. Y. and Mote, C. D., 1995, “On the instability mechanisms of a disk rotating close to a rigid surface”, ASME Journal of Applied Mechanics,

Vol. 62, pp.764 – 771.
[6] Lee, S.-Y, Yoon, D.-W, and Park, K., 2003, “Aerodynamic effect on natural frequency and flutter instability in rotating optical disks”, Microsystem Technologies, Vol.9, pp.369 – 374.
[7] Naganathan, G., Ramadhayani, S. and Bajaj, A. K. 2003, “Numerical simulations of flutter instability of a flexible disk rotating close to a rigid wall”, Journal of Vibration and Control, Vol.9, pp. 95 – 118.
[8] Onagi N., Aman Y., Murata S., and Uchida K., 2004, “High-Density Recording on Air-Stabilized Flexible Optical Disk”, Japanese Journal of Applied Physics, Vol. 43, No. 7B, pp.5009–5013.
[9] Aman Y., Onagi N., Murata S., and Uchida K., 2004, “Effect of Stabilizer in Reducing Effects of Axial Runout on a Flexible Optical Disk”, Japanese Journal of Applied Physics, Vol. 43, No. 7B, pp.4835–4838.
[10] Aman Y., Onagi N., Murata S., and Uchida K., 2005, “Aerodynamic Stabilization of Flexible Optical Disk with Triangularly Arranged Stabilizer System”, Japanese Journal of Applied Physics, Vol. 44, No. 5B, pp.3487–3492.
[11] Aman Y., Onagi N., and Uchida K., 2007, “Aerodynamic stabilization of a flexible optical disk with an asymmetrically and triangularly arranged stabilizer”, Microsystem Technologies, Vol.13, pp.1055–1062.
[12] Kang N. and Raman A., 2006, “Vibrations and stability of a flexible disk rotating in a gas-filled enclosure—Part 1: Theoretical study”, Journal of Sound and Vibration, Vol.296, pp.651–675.
[13] Kang N. and Raman A., 2006, “Vibrations and stability of a flexible disk rotating in a gas-filled enclosure—Part 2: Experimental study”, Journal of Sound and Vibration, Vol.296, pp.676–689.
[14] Gad, A. M. and Rhim, Y. C., 2007, “Study of a Flexible Disk Rotating Close to a Rigid Rotating Wall Considering Fluid Inertia Effects” Journal of Sound and Vibration Vol.317, pp.473-489.
[15] Hoffmann K. A. and Chiang S. T., 1995, “Computational Fluid Dynamics for Engineers”, Engineering Education System, Wichita, Kansas, USA.
[16] Patankar, S. V., 1980, “Numerical Heat Transfer and Fluid Flow”, Hemisphere Publishing Corporation, Taylor & Francis Group, New York.